



This is a repository copy of *13.9% efficiency ternary nonfullerene organic solar cells featuring low-structural order*.

White Rose Research Online URL for this paper:  
<http://eprints.whiterose.ac.uk/156045/>

Version: Accepted Version

---

**Article:**

Du, B., Geng, R., Li, W. et al. (11 more authors) (2019) 13.9% efficiency ternary nonfullerene organic solar cells featuring low-structural order. *ACS Energy Letters*, 4 (10). pp. 2378-2385. ISSN 2380-8195

<https://doi.org/10.1021/acsenergylett.9b01630>

---

This document is the Accepted Manuscript version of a Published Work that appeared in final form in *ACS Energy Letters*, copyright © American Chemical Society after peer review and technical editing by the publisher. To access the final edited and published work see <https://doi.org/10.1021/acsenergylett.9b01630>

**Reuse**

Items deposited in White Rose Research Online are protected by copyright, with all rights reserved unless indicated otherwise. They may be downloaded and/or printed for private study, or other acts as permitted by national copyright laws. The publisher or other rights holders may allow further reproduction and re-use of the full text version. This is indicated by the licence information on the White Rose Research Online record for the item.

**Takedown**

If you consider content in White Rose Research Online to be in breach of UK law, please notify us by emailing [eprints@whiterose.ac.uk](mailto:eprints@whiterose.ac.uk) including the URL of the record and the reason for the withdrawal request.



[eprints@whiterose.ac.uk](mailto:eprints@whiterose.ac.uk)  
<https://eprints.whiterose.ac.uk/>

# 13.9% Efficiency Ternary Nonfullerene Organic Solar Cells Featuring Low-structural Order

Baocai Du<sup>a,b</sup>, Renyong Geng<sup>c</sup>, Wei Li<sup>a,b</sup>, Donghui Li<sup>a,b</sup>, Yuchao Mao<sup>a,b</sup>, Mengxue Chen<sup>a,b</sup>, Xue Zhang<sup>a,b</sup>, Joel A. Smith<sup>d</sup>, Rachel C. Kilbride<sup>d</sup>, Mary E. O’Kane<sup>d</sup>, Dan Liu<sup>a,b</sup>, David G. Lidzey<sup>d</sup>, Weihua Tang<sup>c\*</sup>, Tao Wang<sup>a,b,\*</sup>

<sup>a</sup> School of Materials Science and Engineering, Wuhan University of Technology, Wuhan 430070, China

<sup>b</sup> State Key Laboratory of Silicate Materials for Architectures, Wuhan University of Technology, Wuhan 430070, China

<sup>c</sup> School of Chemical Engineering, Nanjing University of Science and Technology, Nanjing 210094, China

<sup>d</sup> Department of Physics and Astronomy, University of Sheffield, Sheffield, S3 7RH, UK

**ABSTRACT:** The insufficient phase separation between polymer donors and non-fullerene acceptors (NFAs) featuring with low-structural orders disrupts efficient charge transport and increases charge recombination, consequently limits the maximum achievable power conversion efficiency (PCE) of organic solar cells (OSCs). Herein, an NFA IT-M has been added as the third component into the PBDB-T:m-INPOIC OSCs, and is shown to effectively tune the phase separation between donor and acceptor molecules, although all components in the ternary system exhibit low degrees of structural orders. The incorporation of 10 wt% IT-M into a PBDB-T:m-INPOIC binary host blend appreciably increases the length scale of phase separation, creating continuous pathways which increase and balance charge transport. This leads to an enhanced photovoltaic performance from 12.8% in the binary cell to 13.9% for the ternary cell with simultaneously improved open-circuit voltage, short-circuit current and fill factor. This work highlights the beneficial role of ternary components in controlling the morphology of the active layer for high performance OSCs.

Over the past few years, the development of non-fullerene acceptors (NFAs) has driven the impressive progress of organic solar cells (OSCs).<sup>1-4</sup> The tunable energy levels and absorption spectra of NFAs can allow for control of complementary absorption and low voltage loss which are critical for high power conversion efficiency (PCE)<sup>5-8</sup>, with over 16% PCE achieved for single-junction binary non-fullerene OSCs.<sup>9-11</sup> Whilst the emergence of new electron donor and acceptor materials is the primary motivation to further advance OSCs, compositional and morphological optimization within the photoactive layer is vital to realize closer to the theoretical maximum PCE.<sup>10-12</sup> The desired morphology of the photoactive layer should resemble nanoscale phase separated domains for efficient exciton diffusion and dissociation, of the order of the limited exciton diffusion lengths which are usually not more than 10 nm.<sup>15-17</sup> Furthermore bicontinuous networks are favorable for charge carrier transport, collection and suppression of bimolecular recombination.<sup>12,18,19</sup>

Most of the polymer donors, e.g. PTB7-Th and PBDB-T, exhibit low-structural order in the form of  $\pi$ - $\pi$  stacking, due to the confinement of bulky conjugated repeating units in a macromolecular structure.<sup>20,21</sup> The versatile chemical structures of NFAs endow this class of fascinating electron acceptors with very different molecular packing behaviors. For instance, COi8DFIC and INPIC-4F show a high tendency to crystallize into lamellae<sup>22-25</sup>, whilst ITIC and IEICO series materials exhibit  $\pi$ - $\pi$  stacking only<sup>26,27</sup>. NFAs with similar chemical structures to conjugated polymers leads to good miscibility between donors and acceptors, especially with those of low structural orders; however this commonly results in insufficiently separated phases after solution casting, which impacts charge generation, transport and recombination.<sup>28-30</sup> Whereas the fine phase separation and intimate contact between donors and acceptors benefits exciton dissociation, these morphologies are not ideal for charge transport.

Although good efficiencies have been achieved in those photovoltaic systems featuring low structural orders, e.g. PBDB-T:ITIC and PBDB-T:IT-M, further enhancement of performance has proved rather difficult. For example, thermal annealing of PBDB-T:IT-M blend films barely increases the structural orders of PBDB-T and IT-M, explained by their intrinsic low ability to self-organize. Consequently less than 10% PCE improvement has been obtained for annealed

devices compared with as-cast devices.<sup>31</sup> Solvent vapor annealing (SVA) is another effective approach that has been demonstrated to reorganize molecular packing within blends and improve the efficiency of many fullerene-based OSCs.<sup>32,33</sup> However, in non-fullerene OSCs featuring low-structural orders e.g. PTB7-Th:ITIC, only minor enhancement of molecular packing has been observed using a range of solvent or solvent mixture vapors to anneal devices, as such a PCE increase of only 10% can be achieved.<sup>34</sup>

Ternary photovoltaic solar cells prepared by incorporating a third component into conventional binary solar cells have emerged as a promising strategy for realizing further improvements in efficiency.<sup>35-37</sup> This method is favourable as it removes the time-consuming and expensive process of synthesizing new conjugated polymers. Whilst the primary advantage of the ternary strategy is to achieve complementary light absorption<sup>37-39</sup>, it can also effectively regulate the morphology.<sup>40,41</sup> Although literature reports have demonstrated reduced trap density and recombination in ternary systems compared to binary systems,<sup>42-45</sup> less attention has been paid to tuning the phase separation and efficiency of non-fullerene OSCs featuring low structural orders.

In this work, we employ the non-fullerene acceptor IT-M as the third component to tune the domain size in PBDB-T:m-INPOIC blends, which have until now been inhibited by insufficient phase separation, as all components exhibit low-structural orders. The presence of an intermediate amount of IT-M enhances photon absorption in the ternary device. The appreciatively enlarged length scale of phase separation induced by the presence of 10 wt% IT-M facilitates increased and balanced charge mobilities with minimized trap-assisted recombination. As a result, the ternary OSC achieves a maximum PCE of 13.9% compared with 12.8% for the PBDB-T:m-INPOIC binary OSC, with the simultaneously increased device metrics of  $V_{oc}$  of 0.86 V,  $J_{sc}$  of 22.2 mA/cm<sup>2</sup> and FF of 71.3%. This work highlights the beneficial role of ternary components in mediating morphology of the active layer to improve device performance.

The chemical structures, energy levels of materials and schematic of the device structure used in this work are shown in **Figure 1a-b**.<sup>46,47</sup> **Figure 1c** clearly shows the complementary absorption of the different components in the ternary system. To examine the possible Förster resonance energy transfer (FRET) between m-INPOIC and IT-M, we have measured the photoluminescence (PL)

spectra of the individual components and their mixtures with different weight ratios. As shown in **Figure 1d**, IT-M and m-INPOIC exhibit distinct emission peaks at 765 and 873 nm respectively. The broad overlap between the emission spectrum of IT-M and the absorption spectrum of m-INPOIC (**Figure 1c**) should enable efficient energy transfer from IT-M to m-INPOIC. In the m-INPOIC:IT-M blend, the emission signal of IT-M is markedly quenched with a single emissive peak observed at 873 nm that is associated with m-INPOIC, suggesting efficient energy transfer from IT-M to m-INPOIC which is favorable for photovoltaic performance.<sup>48</sup> From this efficient energy transfer process we can also imply there is good miscibility between these two acceptors, with close mixing in the blend film.<sup>35,41,49</sup>

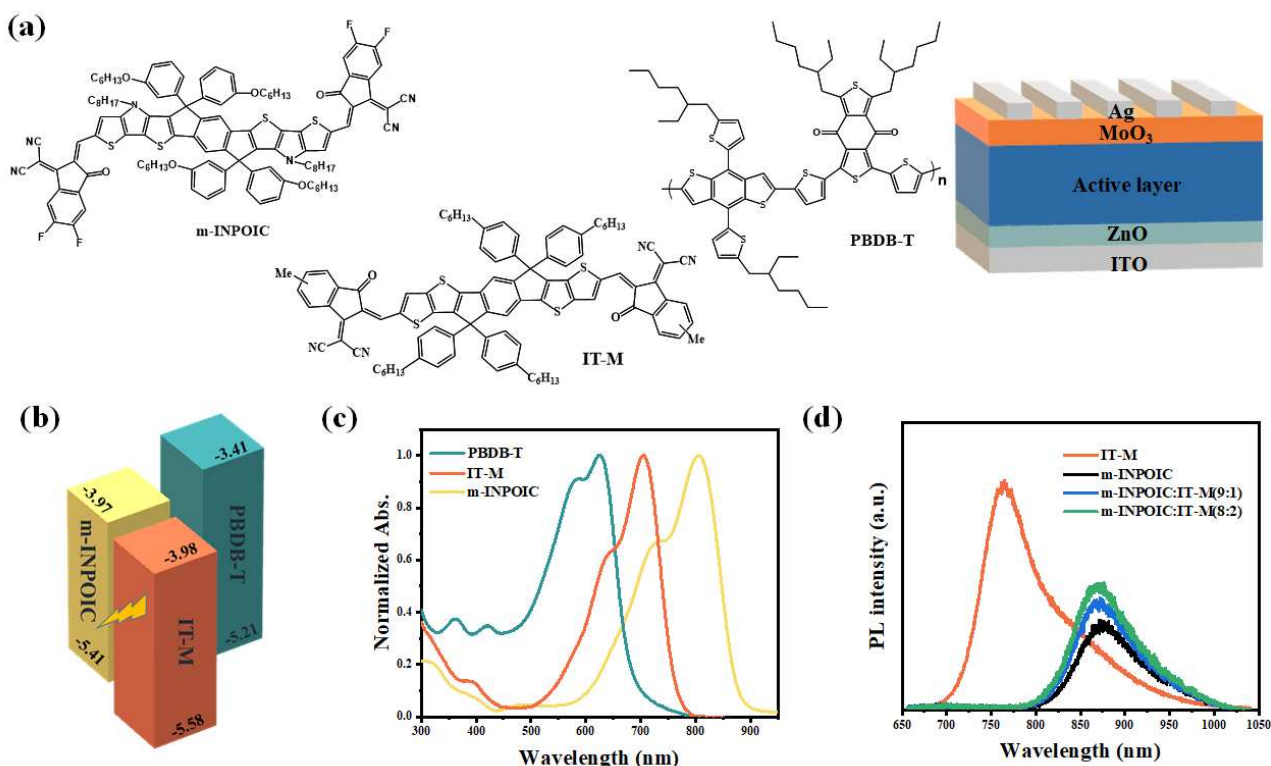


**Figure 1.** (a) Chemical structures of polymer donor and non-fullerene acceptors, and the device architecture used in this work. (b) Schematic energy diagrams of PBDB-T, IT-M and m-INPOIC, here the lightning bolt indicates the related energy transfer process. (c) Optical absorption spectra of neat films of PBDB-T, m-INPOIC and IT-M. (d) PL spectra of m-INPOIC, IT-M and their mixtures at the weight ratios of 9:1 and 8:2, excited with a 532 nm laser.

Transmission electron microscopy (TEM) was performed to understand the phase separated domain size within the binary and ternary blends. As shown in **Figure 2a-c**, the dark and bright

regions represent the acceptor and donor domains respectively, because of their different electron densities.<sup>50</sup> The TEM image of the PBDB-T:m-INPOIC binary film (see **Figure 2a**) shows fine mixing and homogeneous distribution of donors and acceptors, whilst the continuous domain networks are less pronounced. Upon the incorporation of IT-M (see **Figure 2b** and **c**), the distinction between dark and bright regions becomes more pronounced. This suggests increased phase separation leading to larger and purer domains within the ternary blend, which will help the formation of bicontinuous paths for efficient charge transport and reduced charge recombination.<sup>18,19</sup> These larger domains will have higher charge mobility because of the much faster carrier transport within a single-phase domain than between domains.<sup>51</sup>

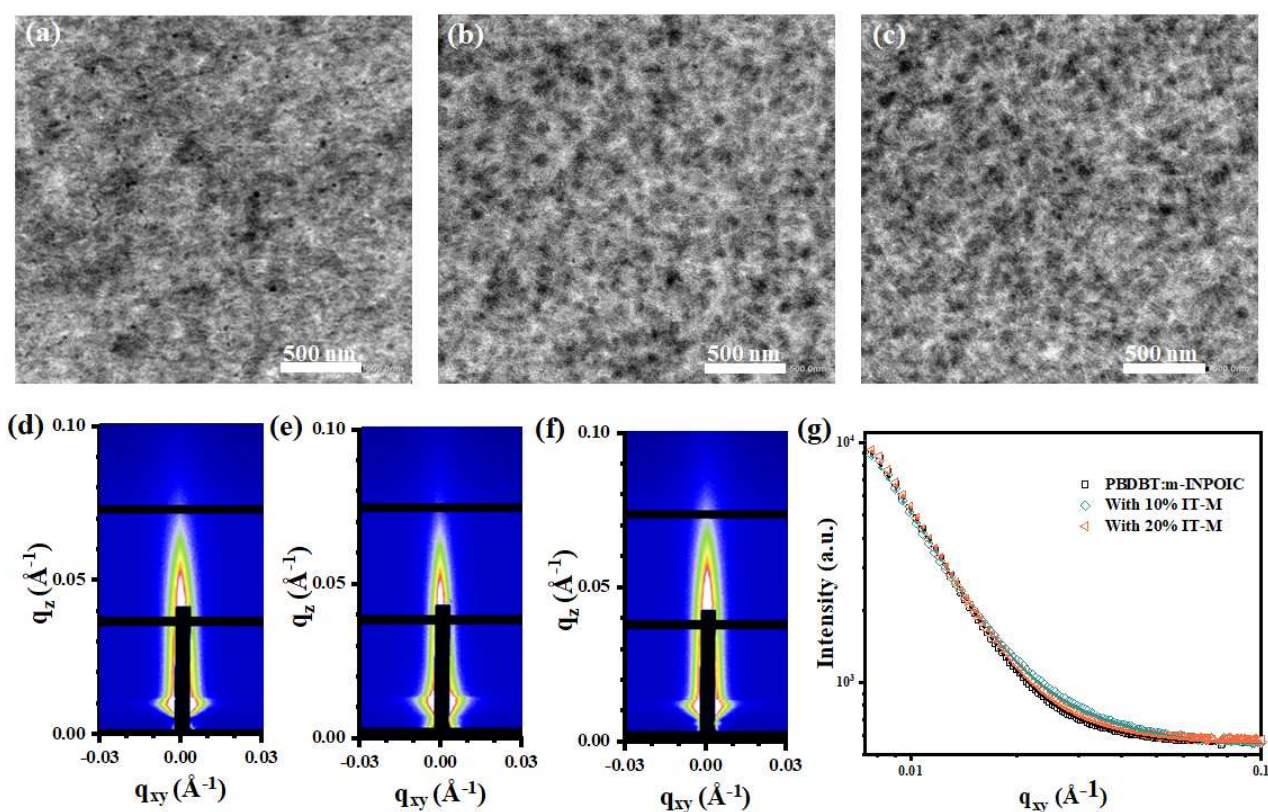


**Figure 2.** TEM images of (a) PBDB-T:m-INPOIC film, and its ternary blends with (b) 10%, (c) 20% IT-M. 2D GISAXS patterns of (d) PBDB-T:m-INPOIC, and its ternary blends with (e) 10% IT-M, (f) 20% IT-M. (g) 1D GISAXS profiles along the  $q_{xy}$  axis for PBDB-T:m-INPOIC blend films with different IT-M contents.

In order to quantify the phase separated domain sizes of donors and acceptors, grazing-incidence small-angle X-ray scattering (GISAXS) was employed. The corresponding 2D GISAXS patterns of binary and ternary blends and their 1D GISAXS profiles along  $q_{xy}$  axis are

shown in **Figure 2d-g**. A universal model (detailed in the supporting information) was used to fit the 1D profiles and the relevant fitting parameters are shown in **Table 1**. Here the correlation length ( $\xi$ ) refers to the domain size of the PBDB-T-rich phase,  $\eta$  and  $D$  represent the correlation length and fractal dimension of acceptors and  $2R_g$  (the product of  $\eta$  and  $D$ ) is regarded as the domain size of acceptor aggregation. According to **Table 1**, the PBDB-T and m-INPOIC domain sizes in the binary blend are 13.3 and 32.1 nm respectively. Adding 10 wt% IT-M into binary blend leads to the growth of both PBDB-T and m-INPOIC domains, which are enlarged to 14.8 and 35.0 nm respectively. Further increased domain size and phase separation were observed when 20 wt% IT-M was added. Therefore, we conclude the addition of IT-M increases the domain size of both donors and acceptors. The ternary blend with 10 wt% IT-M shows the smallest fractal dimension of 2.6, suggesting loosely packed aggregates of m-INPOIC, which could extend to larger regions facilitating both exciton dissociation and charge transport.<sup>52,53</sup> This quantitative observation is consistent with the more pronounced contrast and domain size within the TEM images of the ternary blends.

**Table 1.** Fitting parameters of 1D GISAXS profiles for PBDB-T:m-INPOIC and its ternary films.

	$\xi$ (nm)	$\eta$ (nm)	$D$	$2R_g$ (nm)
PBDB-T:m-INPOIC	13.3	13.9	2.8	32.1
With 10% IT-M	14.8	16.2	2.6	35.0
With 20% IT-M	16.0	16.7	2.9	39.7

Due to the competition between phase separation and molecular ordering,<sup>29</sup> we further investigate the effect of the addition of the third component IT-M on the molecular packing and orientation via grazing incidence wide-angle X-ray scattering (GIWAXS) measurements. The 2D diffraction patterns and 1D profiles are shown in **Figure 3**. It is immediately apparent in the 2D GIWAXS patterns that the face-on  $\pi$ - $\pi$  stacking of the blends is gradually enhanced upon the incorporation of IT-M. As shown in **Figure 3d-e**, the binary PBDB-T:m-INPOIC film shows a weak and broad  $\pi$ - $\pi$  peak in the out-of-plane (OOP) direction and a sharp lamellar stacking in the in-plane (IP) direction, which is the character of preferential face-on orientation.<sup>54</sup> Deconvolution of this

broad  $\pi$ - $\pi$  peak gives two convolved peaks located at  $q_z \approx 1.73 \text{ \AA}^{-1}$  and  $q_z \approx 1.80 \text{ \AA}^{-1}$  (see in **Figure S1**), which can be assigned to PBDB-T and m-INPOIC components respectively.<sup>47</sup> With the addition of IT-M, no obvious diffraction peaks from IT-M were observed, which is consistent with the low structural order of IT-M.<sup>31</sup> Meanwhile, stronger  $\pi$ - $\pi$  stacking diffraction in the OOP direction and PBDB-T lamellar stacking in the IP direction were observed in **Figure 3b** and **c**. Deconvolution of these broad  $\pi$ - $\pi$  peaks from 1.60 to 1.90  $\text{\AA}^{-1}$  using multi-Gaussian peak fitting is shown in **Figure S1**. With the addition of IT-M, the  $\pi$ - $\pi$  peak positions of PBDB-T and m-INPOIC slightly shift to higher  $q$  values, suggesting a tighter stacking distance. Comparing the intensity changes of the deconvoluted peaks, the main contribution to the enhanced  $\pi$ - $\pi$  stacking comes from PBDB-T in the ternary blend, with negligible changes of m-INPOIC. This suggests enhanced ordering of PBDB-T, which is most pronounced with the addition of 20 wt% IT-M. We regard this enhanced ordering as resulting from the increased domain size within the ternary blends, allowing PBDB-T molecules to pack efficiently without the interruption of acceptor molecules. The fact that the  $\pi$ - $\pi$  stacking intensity of m-INPOIC barely changes suggests the good miscibility between m-INPOIC and IT-M, which might form an alloy as observed in many ternary systems.<sup>55,56</sup> The increased packing of PBDB-T in the OOP direction within the slightly larger domains will increase the hole mobility (results presented in a later section) to facilitate carrier transport along the vertical direction towards the anode.<sup>57</sup>

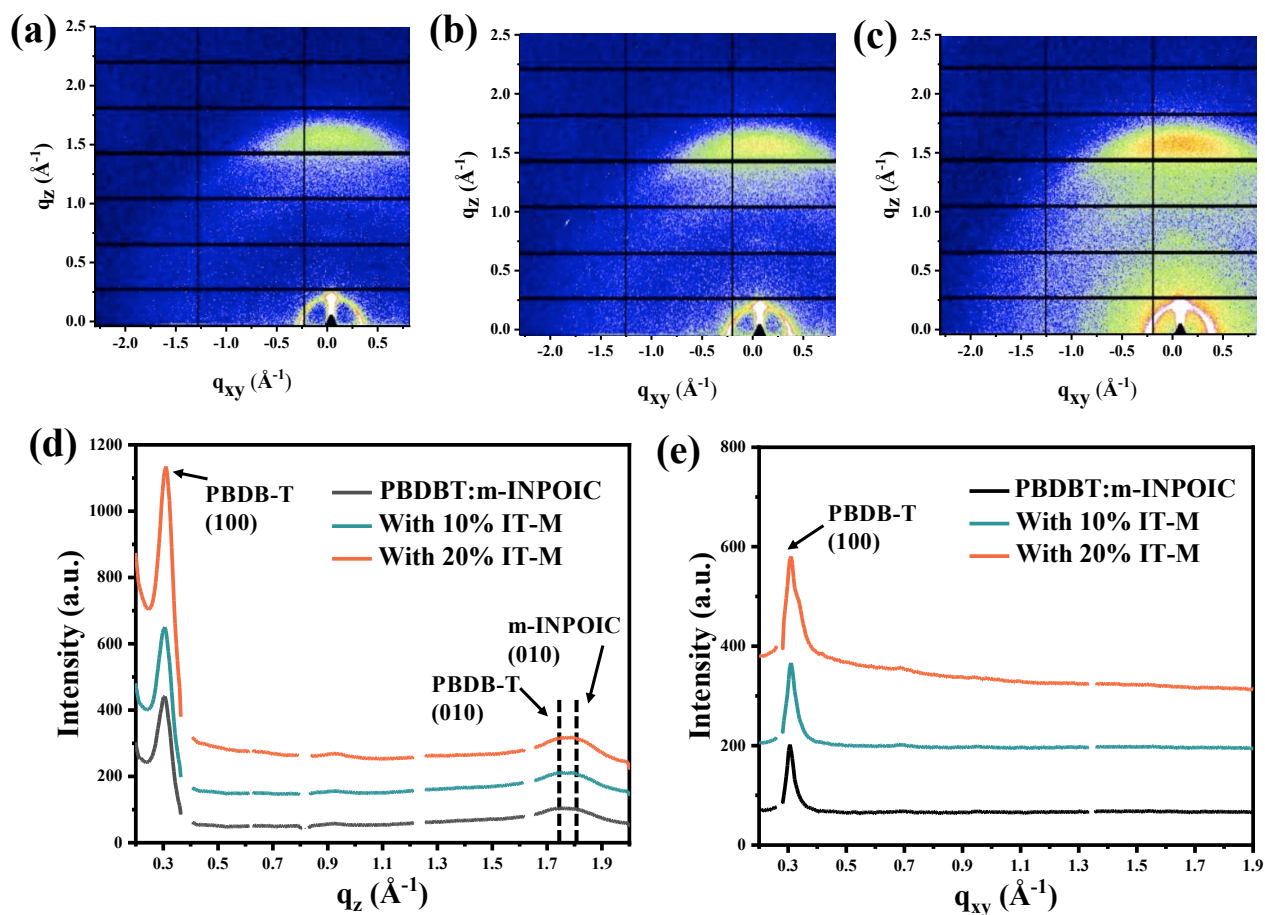


**Figure 3.** 2D GIWAXS patterns of (a) PBDB-T:m-INPOIC film, and its ternary blends with (b) 10 wt%, (c) 20 wt% IT-M. Corresponding (d) out-of-plane and (e) in-plane 1D profiles of GIWAXS patterns along the  $q_z$ - and  $q_{xy}$ -axis.

It is well accepted that the efficiency of OSCs is greatly related to the photon absorption of the photoactive layer.<sup>27</sup> Thus we further investigated the absorption spectra of the binary and ternary films where the overall donor/acceptor weight ratio was kept at 1:1. Referring to the absorption spectra in **Figure 4a**, the prominent peaks at 635 and 800 nm correspond to the absorption of PBDB-T and m-INPOIC respectively. With the addition of IT-M, the absorption is enhanced in the wavelength range from 500 to 700 nm. We attribute this to two reasons, firstly the stronger absorption of IT-M in this range, and secondly the enhanced molecular packing of PBDB-T (discussed above in the GIWAXS section) which will also enhance photon absorption.<sup>29</sup> With the addition of 20 wt% IT-M, however, the absorption at longer wavelengths reduces notably, which results from the reduced fraction of m-INPOIC in the blend.

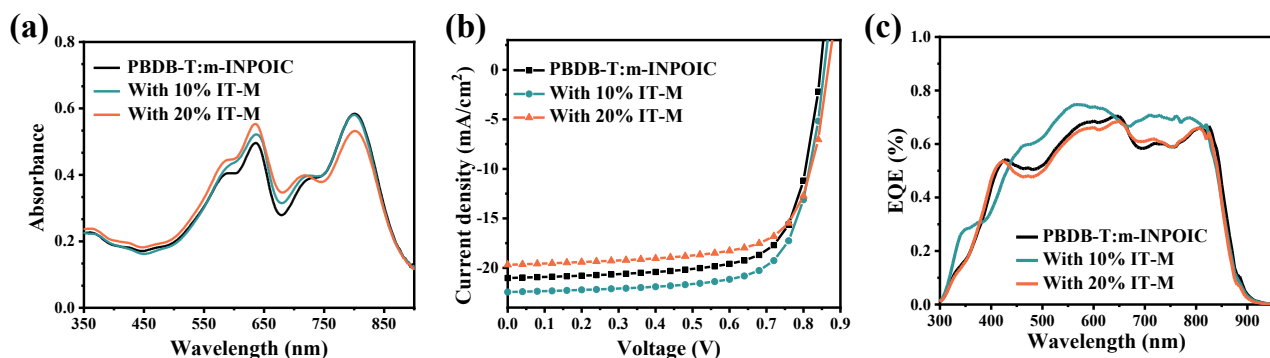


**Figure 4.** (a) Absorbance of PBDB-T:m-INPOIC films with different IT-M contents, (b) Champion J–V curves, and (c) EQE of devices fabricated with different IT-M contents.

**Table 2.** The photovoltaic parameters of PBDB-T:m-INPOIC OSCs with varying IT-M content obtained under simulated AM 1.5 G illumination at 100 mW/cm<sup>2</sup>. The statistical data were obtained from over 20 individual devices.

	FF [%]	J <sub>sc</sub> [mA cm <sup>-2</sup> ]	Cal. J <sub>sc</sub> [mA cm <sup>-2</sup> ]	V <sub>oc</sub> [V]	PCE <sub>avg</sub> (PCE <sub>max</sub> ) [%]
PBDB-T:m-INPOIC	70.8±0.45	20.7±0.30	19.6	0.85±0.002	12.5±0.26 (12.8)
With 10% IT-M	71.3±0.66	22.2±0.24	21.0	0.86±0.003	13.7±0.16 (13.9)
With 20% IT-M	72.4±0.85	19.1±0.43	18.2	0.87±0.004	11.9±0.16 (12.2)

A series of inverted binary and ternary devices were fabricated to evaluate the effects of these morphological characteristics on device performance. The overall donor to acceptor ratio was kept constant at 1:1 in this work. The J–V curves of best-performing devices are shown in **Figure 4b** and the device metrics for each composition are summarized in **Table 2**. The control device refers to the PBDB-T:m-INPOIC binary cell, which exhibits a PCE<sub>max</sub> of 12.8%, with a FF of 70.8%, a J<sub>sc</sub> of 20.7 mAcm<sup>-2</sup> and a V<sub>oc</sub> of 0.85 V. Incorporating 10 wt% IT-M into the PBDB-T:m-INPOIC blend leads to simultaneous improvements of the J<sub>sc</sub> to 22.2 mAcm<sup>-2</sup>, FF to 71.3% and V<sub>oc</sub> to 0.86V, resulting in a PCE<sub>max</sub> of 13.9%. The larger domain sizes in the ternary OSCs will facilitate charge carrier transport, on the other hand, the reduced D/A interface area and the longer distance that excitons have to migrate are harmful to efficient exciton dissociation.<sup>16</sup> As a result, when 20 wt% IT-M was incorporated to generate domains with excessive sizes, the FF of the device further

increases to 72.4% and the  $V_{oc}$  increases to 0.87V, but the  $J_{sc}$  decreases abruptly to 19.1 mAcm<sup>-2</sup>, leading to a low  $PCE_{max}$  of 12.2% only. In general, the  $V_{oc}$  of the device is associated with the offsets between the highest occupied molecule orbital (HOMO) of the donor and the lowest unoccupied molecule orbital (LUMO) of the acceptor.<sup>58,59</sup> Here, the gradually increasing  $V_{oc}$  is in line with the IT-M content, suggesting that IT-M acts as an energy-level modulator to monotonically elevate the LUMO levels of the mixed acceptors due to its higher-lying LUMO.

The external quantum efficiency (EQE) spectra of the best-performing devices are shown in **Figure 4c**. When the binary blend had 10 wt% IT-M added, the EQE spectra of the device shows marked increase in the broad region between 450 and 800 nm, which is consistent with the enhanced absorption in this region. Significantly increased charge dissociation and collection as well as suppressed recombination account for the improved EQE values (discussed below). Further increasing the content of IT-M to 20% leads to slightly reduced photon to current efficiency from 450 to 650 nm. This indicates that excessive amount of IT-M begins to hamper current generation due to inefficient generation of free charges from excitons, because of sub-optimal phase separation.

To further investigate the effect of the varying degree of phase separation on exciton dissociation and collection, the photocurrent density ( $J_{ph}$ ) as a function of the effective voltage ( $V_{eff}$ ) were measured, as shown in **Figure 5a**.<sup>60</sup> Here  $J_{ph} = J_L - J_D$ , in which  $J_L$  and  $J_D$  are the photocurrent densities under illumination and dark respectively.  $V_{eff} = V_o - V_a$ , where  $V_o$  is the voltage when  $J_L = J_D$  and  $V_a$  is the applied voltage. Assuming that all the generated excitons have dissociated and been collected by electrodes at large  $V_{eff}$ , a saturated photocurrent density ( $J_{sat}$ ) will be reached. The maximum  $J_{sat}$  of the ternary device with 10 wt% IT-M is partly due to the efficient energy transfer from IT-M to m-INPOIC. The exciton dissociation possibility ( $P_{diss}$ ) and charge collection efficiency ( $P_{coll}$ ) are defined as  $J_{ph}/J_{sat}$  values under short-circuit condition and maximal power output condition respectively. As displayed in **Table 3**, the  $P_{diss}$  values of the ternary OSC with 10% IT-M content is higher than the binary OSC. But at the higher amount of 20 wt% IT-M, excessive phase separation and reduced D/A interfaces results in the inhibition of exciton dissociation. The dramatically increased  $P_{coll}$  for 10% IT-M is attributed to the more ordered molecular packing of

PBDB-T and the formation of bicontinuous networks, enabling efficient charge carrier transport with suppressed carrier recombination.

Additionally, we took J-V measurements of OSCs under different light intensity ( $P_{\text{light}}$ ) to gain more insight into the charge recombination behavior of devices. The profiles of  $J_{\text{sc}}$  and  $V_{\text{oc}}$  as a function of light intensity ( $P_{\text{light}}$ ) are described in **Figure 5b** and c. By analyzing the  $V_{\text{oc}}$  versus  $\ln(P_{\text{light}})$  plot, the dominant charge recombination mechanism can be distinguished. At the bimolecular recombination condition, the slope of  $V_{\text{oc}}$  versus  $\ln(P_{\text{light}})$  is close to  $KT/q$ , where  $K$  is the Boltzmann constant,  $T$  is the absolute temperature and  $q$  is the elementary charge. The slope will be larger than  $KT/q$  for trap-assisted recombination. The slope of  $V_{\text{oc}}$  versus  $\ln(P_{\text{light}})$  for the binary device is  $1.32 KT/q$ , which decreases to  $1.21 KT/q$  and  $1.28 KT/q$  for ternary devices with 10% and 20% IT-M respectively, suggesting the most effectively suppressed trap-assistance recombination with the addition of 10% IT-M. Meanwhile, the slopes of  $\log(J_{\text{sc}})$  versus  $\log(P_{\text{light}})$  plots were analyzed to evaluate the degree of bimolecular recombination. As shown in **Figure 5c**, the slopes are 0.96, 0.98 and 0.96 for the binary and ternary devices with 10% IT-M and 20% IT-M, respectively. A slope close to unity signifies that bimolecular recombination dominates in these devices.

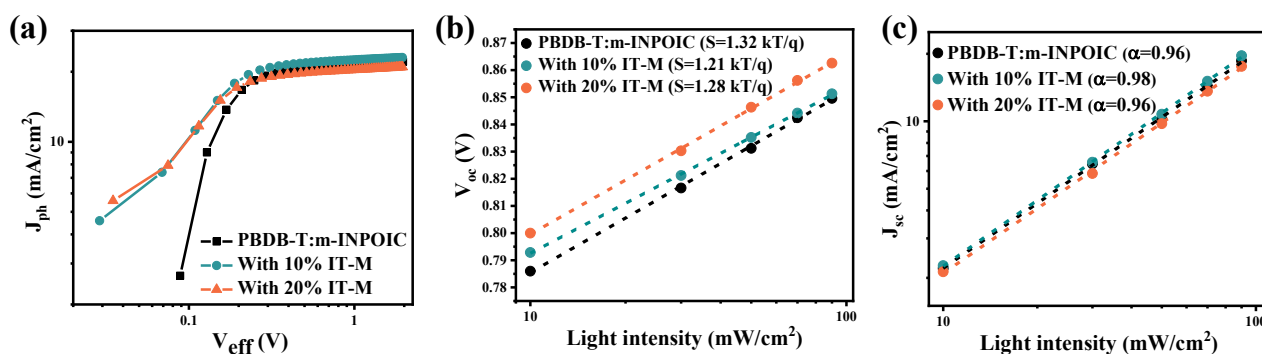


**Figure 5.** (a) Photocurrent density ( $J_{\text{ph}}$ ) versus effective voltage ( $V_{\text{eff}}$ ) curves. (b) Dependence of  $V_{\text{oc}}$  on light intensity and (c) dependence of  $J_{\text{sc}}$  on light intensity for the devices with different amounts of IT-M.

We finally investigated the effect of IT-M on carrier mobilities ( $\mu$ ) using the space charge limited current (SCLC) method. The hole- and electron- only devices were fabricated with the structures of ITO/PEDOT:PSS/active layer/MoO<sub>3</sub>/Ag and ITO/ZnO/active layer/Ca/Ag,

respectively. The  $J^{1/2}$ - $V$  curves are shown in **Figure S2**, and the mobilities are extracted and summarized in **Table 3**. The  $\mu_h$  and  $\mu_e$  of the PBDB-T:m-INPOIC binary device are  $2.6 \times 10^{-4} \text{ cm}^2 \text{ V}^{-1} \text{ s}^{-1}$  and  $2.1 \times 10^{-4} \text{ cm}^2 \text{ V}^{-1} \text{ s}^{-1}$  respectively. After the incorporation of 10% IT-M, the ternary device displays higher  $\mu_h$  and  $\mu_e$  of  $2.8 \times 10^{-4} \text{ cm}^2 \text{ V}^{-1} \text{ s}^{-1}$  and the hole and electron transport becomes balanced as determined by the  $\mu_h/\mu_e$  ratio of unity. The enhanced molecular order of PBDB-T and improved bicontinuous pathways account for these increased mobilities. As more IT-M was added,  $\mu_h$  continuously increases to  $4.2 \times 10^{-4} \text{ cm}^2 \text{ V}^{-1} \text{ s}^{-1}$  and  $\mu_e$  increases to  $3.0 \times 10^{-4} \text{ cm}^2 \text{ V}^{-1} \text{ s}^{-1}$ , thus the  $\mu_h/\mu_e$  becomes unbalanced, which will increase charge accumulation and recombination, worsening device performance.

**Table 3.**  $J_{\text{sat}}$ ,  $P_{\text{diss}}$ ,  $P_{\text{coll}}$ , hole and electron mobilities of PBDB-T:m-INPOIC and its ternary OSCs with different contents of IT-M.

IT-M content	$J_{\text{sat}}$ [mA cm <sup>-2</sup> ]	$P_{\text{diss}}$	$P_{\text{coll}}$	Hole mobility ( $\mu_h$ ) [cm <sup>2</sup> V <sup>-1</sup> s <sup>-1</sup> ]	Electron mobility ( $\mu_e$ ) [cm <sup>2</sup> V <sup>-1</sup> s <sup>-1</sup> ]	$\mu_h/\mu_e$
0%	22.1	97.5%	83.3%	$2.6 \times 10^{-4}$	$2.1 \times 10^{-4}$	1.2
10%	22.9	98.3%	88.8%	$2.8 \times 10^{-4}$	$2.8 \times 10^{-4}$	1.0
20%	20.9	97.2%	86.9%	$4.2 \times 10^{-4}$	$3.0 \times 10^{-4}$	1.4

In summary, PBDB-T:m-INPOIC binary non-fullerene OSCs with a maximum PCE of 12.8% were enhanced to 13.9% PCE by employing 10 wt% IT-M (relative to the acceptor) as a ternary component, with simultaneously increased  $J_{\text{sc}}$ , FF and  $V_{\text{oc}}$ . Morphological studies show appreciably enlarged phase domain size via the addition of IT-M, helping to increase the molecular packing of PBDB-T, as well as creating continuous donor and acceptor networks for efficient charge transport towards the respective electrodes. The optimized morphology via tuning of the phase separation of the ternary system leads to increased light absorption and charge mobility, balanced charge transport and suppressed carrier recombination. We have there demonstrated that ternary component implementation is an effective strategy to prepare high-performance ternary non-fullerene OSCs consisting of components with low structural orders.

## ASSOCIATED CONTENT

### Supporting information

Materials, fabrication and characterization of OSCs, mobility calculation, GIWAXS and GISAXS fitting details and data.

## AUTHOR INFORMATION

### Corresponding Authors

\*E-mail: [twang@whut.edu.cn](mailto:twang@whut.edu.cn) (T. Wang).

\*E-mail: [whtang@njust.edu.cn](mailto:whtang@njust.edu.cn) (W. Tang).

### ORCID

Tao Wang: 0000-0002-5887-534X

Weihua Tang: 0000-0002-6233-3471

### Notes

The authors declare no competing financial interest.

## ACKNOWLEDGMENTS

This work was supported by the National Natural Science Foundation of China (Grant No. 21774097) and the Natural Science Foundation of Hubei Province (Grant No. 2018CFA055) of China. All authors thank the beamline BL16B1 at Shanghai Synchrotron Radiation Facility (China) for providing the beam time and help during experiment. We also thank the Diamond Light Source (UK) beamline I07 where GIWAXS measurements were performed (via beamtime allocation SI22651-1). We also thank the U.K. EPSRC for funding studentships for R.C.K. (DTG allocation), M.E.O’K. (EP/L016281/1: CDT in Polymers, Soft Matter and Colloids) and J.A.S. (EP/L01551X/1: CDT in New and Sustainable PV).

## REFERENCES

- (1) Hou, J.; Inganäs, O.; Friend, R. H.; Gao, F. Organic Solar Cells Based on Non-Fullerene Acceptors. *Nat. Mater.* **2018**, *17*, 119–128.

- (2) Cheng, P.; Li, G.; Zhan, X.; Yang, Y. Next-Generation Organic Photovoltaics Based on Non-Fullerene Acceptors. *Nat. Photonics* **2018**, *12*, 131–142.
- (3) Yan, C.; Barlow, S.; Wang, Z.; Yan, H.; Jen, A. K. Y.; Marder, S. R.; Zhan, X. Non-Fullerene Acceptors for Organic Solar Cells. *Nat. Rev. Mater.* **2018**, *3*, 18003.
- (4) Fu, H.; Wang, Z.; Sun, Y. Polymer Donors for High-Performance Non-Fullerene Organic Solar Cells. *Angew. Chem. Int. Ed.* **2019**, *58*, 4442–4453.
- (5) Xu, Y.; Yao, H.; Hou, J. Recent Advances in Fullerene-Free Polymer Solar Cells: Materials and Devices. *Chinese J. Chem.* **2019**, *37*, 207–215.
- (6) Chen, W.; Zhang, Q. Recent Progress in Non-Fullerene Small Molecule Acceptors in Organic Solar Cells (OSCs). *J. Mater. Chem. C* **2017**, *5*, 1275–1302.
- (7) Eftaiha, A. F.; Sun, J.-P.; Hill, I. G.; Welch, G. C. Recent Advances of Non-Fullerene, Small Molecular Acceptors for Solution Processed Bulk Heterojunction Solar Cells. *J. Mater. Chem. A* **2014**, *2*, 1201–1213.
- (8) Lu, L.; Zheng, T.; Wu, Q.; Schneider, A. M.; Zhao, D.; Yu, L. Recent Advances in Bulk Heterojunction Polymer Solar Cells. *Chem. Rev.* **2015**, *115*, 12666–12731.
- (9) Cui, Y.; Yao, H.; Zhang, J.; Zhang, T.; Wang, Y.; Hong, L.; Xian, K.; Xu, B.; Zhang, S.; Peng, J.; et al. Over 16% Efficiency Organic Photovoltaic Cells Enabled by a Chlorinated Acceptor with Increased Open-Circuit Voltages. *Nat. Commun.* **2019**, *10*, 2515.
- (10) Xu, X.; Feng, K.; Bi, Z.; Ma, W.; Zhang, G.; Peng, Q. Single-Junction Polymer Solar Cells with 16.35% Efficiency Enabled by a Platinum(II) Complexation Strategy. *Adv. Mater.* **2019**, *31*, 1901872.
- (11) Fan, B.; Zhang, D.; Li, M.; Zhong, W.; Zeng, Z.; Ying, L.; Huang, F.; Cao, Y. Achieving over 16% Efficiency for Single-Junction Organic Solar Cells. *Sci. China Chem.* **2019**, *62*, 746–752.
- (12) Yan, T.; Song W.; Huang J.; Peng R.; Huang L.; Ge Z. 16.67% Rigid and 14.06% Flexible Organic Solar Cells Enabled by Ternary Heterojunction Strategy. *Adv. Mater.* **2019**, DOI: 10.1002/adma.201902210.

- (13) Rivnay, J.; Mannsfeld, S. C. B.; Miller, C. E.; Salleo, A.; Toney, M. F. Quantitative Determination of Organic Semiconductor Microstructure from the Molecular to Device Scale. *Chem. Rev.* **2012**, *112*, 5488–5519.
- (14) Gurney, R. S.; Lidzey, D. G.; Wang, T. A Review of Non-Fullerene Polymer Solar Cells: From Device Physics to Morphology Control. *Rep. Prog. Phys.* **2019**, *82*, 036601.
- (15) Duong, D. T.; Walker, B.; Lin, J.; Kim, C.; Love, J.; Purushothaman, B.; Anthony, J. E.; Nguyen, T. Q. Molecular Solubility and Hansen Solubility Parameters for the Analysis of Phase Separation in Bulk Heterojunctions. *J. Polym. Sci. Part B Polym. Phys.* **2012**, *50*, 1405–1413.
- (16) Stoltzfus, D. M.; Donaghey, J. E.; Armin, A.; Shaw, P. E.; Burn, P. L.; Meredith, P. Charge Generation Pathways in Organic Solar Cells: Assessing the Contribution from the Electron Acceptor. *Chem. Rev.* **2016**, *116*, 12920–12955.
- (17) Clarke, T. M.; Durrant, J. R. Charge Photogeneration in Organic Solar Cells. *Chem. Rev.* **2010**, *110*, 6736–6767.
- (18) Jaquith, M.; Muller, E. M.; Marohn, J. A. Time-Resolved Electric Force Microscopy of Charge Trapping in Polycrystalline Pentacene. *J. Phys. Chem. B* **2007**, *111*, 7711–7714.
- (19) Ma, W.; Kim, J. Y.; Lee, K.; Heeger, A. J. Effect of the Molecular Weight of Poly(3-Hexylthiophene) on the Morphology and Performance of Polymer Bulk Heterojunction Solar Cells. *Macromol. Rapid Commun.* **2007**, *28*, 1776–1780.
- (20) Liao, S.-H.; Jhuo, H.-J.; Cheng, Y.-S.; Chen, S.-A. Fullerene Derivative-Doped Zinc Oxide Nanofilm as the Cathode of Inverted Polymer Solar Cells with Low-Bandgap Polymer (PTB7-Th) for High Performance. *Adv. Mater.* **2013**, *25*, 4766–4771.
- (21) Qian, D.; Ye, L.; Zhang, M.; Liang, Y.; Li, L.; Huang, Y.; Guo, X.; Zhang, S.; Tan, Z.; Hou, J. Design, Application, and Morphology Study of a New Photovoltaic Polymer with Strong Aggregation in Solution State. *Macromolecules* **2012**, *45*, 9611–9617.
- (22) Li, W.; Chen, M.; Cai, J.; Spooner, E. L. K.; Zhang, H.; Gurney, R. S.; Liu, D.; Xiao, Z.; Lidzey, D. G.; Ding, L.; et al. Molecular Order Control of Non-Fullerene Acceptors for High-Efficiency Polymer Solar Cells. *Joule* **2019**, *3*, 819–833.

- (23) Li, W.; Chen, M.; Zhang, Z.; Cai, J.; Zhang, H.; Gurney, R. S.; Liu, D.; Yu, J.; Tang, W.; Wang, T. Retarding the Crystallization of a Nonfullerene Electron Acceptor for High-Performance Polymer Solar Cells. *Adv. Funct. Mater.* **2018**, *29*, 1807662.
- (24) Xiao, Z.; Jia, X.; Li, D.; Wang, S.; Geng, X.; Liu, F.; Chen, J.; Yang, S.; Russell, T. P.; Ding, L. 26 mA cm<sup>-2</sup> Jsc from Organic Solar Cells with a Low-Bandgap Nonfullerene Acceptor. *Sci. Bull.* **2017**, *62*, 1494–1496.
- (25) Li, H.; Xiao, Z.; Ding, L.; Wang, J. Thermostable Single-Junction Organic Solar Cells with a Power Conversion Efficiency of 14.62%. *Sci. Bull.* **2018**, *63*, 340–342.
- (26) Mai, J.; Xiao, Y.; Zhou, G.; Wang, J.; Zhu, J.; Zhao, N.; Zhan, X.; Lu, X. Hidden Structure Ordering Along Backbone of Fused-Ring Electron Acceptors Enhanced by Ternary Bulk Heterojunction. *Adv. Mater.* **2018**, *30*, 1802888.
- (27) Song, X.; Gasparini, N.; Ye, L.; Yao, H.; Hou, J.; Ade, H.; Baran, D. Controlling Blend Morphology for Ultrahigh Current Density in Nonfullerene Acceptor-Based Organic Solar Cells. *ACS Energy Lett.* **2018**, *3*, 669–676.
- (28) Yang, B.; Zhang, S.; Chen, Y.; Cui, Y.; Liu, D.; Yao, H.; Zhang, J.; Wei, Z.; Hou, J. Investigation of Conjugated Polymers Based on Naphtho[2,3-c]Thiophene-4,9-Dione in Fullerene-Based and Fullerene-Free Polymer Solar Cells. *Macromolecules* **2017**, *50*, 1453–1462.
- (29) Liang, Q.; Han, J.; Song, C.; Yu, X.; Smilgies, D. M.; Zhao, K.; Liu, J.; Han, Y. Reducing the Confinement of PBDB-T to ITIC to Improve the Crystallinity of PBDB-T/ITIC Blends. *J. Mater. Chem. A* **2018**, *6*, 15610–15620.
- (30) Hu, H.; Jiang, K.; Chow, P. C. Y.; Ye, L.; Zhang, G.; Li, Z.; Carpenter, J. H.; Ade, H.; Yan, H. Influence of Donor Polymer on the Molecular Ordering of Small Molecular Acceptors in Nonfullerene Polymer Solar Cells. *Adv. Energy Mater.* **2018**, *8*, 1701674.
- (31) Li, W.; Cai, J.; Yan, Y.; Cai, F.; Li, S.; Gurney, R. S.; Liu, D.; McGettrick, J. D.; Watson, T. M.; Li, Z.; et al. Correlating Three-Dimensional Morphology With Function in PBDB-T:IT-M Non-Fullerene Organic Solar Cells. *Sol. RRL* **2018**, *2*, 1870204..
- (32) Jin, C.; Olsen, B. C.; Lubber, E. J.; Buriak, J. M. Nanopatterning via Solvent Vapor Annealing of Block Copolymer Thin Films. *Chem. Mater.* **2017**, *29*, 176–188.

- (33) Vogelsang, J.; Brazard, J.; Adachi, T.; Bolinger, J. C.; Barbara, P. F. Watching the Annealing Process One Polymer Chain at a Time. *Angew. Chem. Int. Ed.* **2011**, *50*, 2257–2261.
- (34) S. Gurney, R.; Li, W.; Yan, Y.; Liu, D.; J. Pearson, A.; Wang, T. Morphology and Efficiency Enhancements of PTB7-Th:ITIC Nonfullerene Organic Solar Cells Processed via Solvent Vapor Annealing. *J. Energy Chem.* **2019**, *37*, 148–156.
- (35) An, Q.; Zhang, F.; Zhang, J.; Tang, W.; Deng, Z.; Hu, B. Versatile Ternary Organic Solar Cells: A Critical Review. *Energy Environ. Sci.* **2016**, *9*, 281–322.
- (36) Huang, W.; Cheng, P.; Yang, Y. M.; Li, G.; Yang, Y. High-Performance Organic Bulk-Heterojunction Solar Cells Based on Multiple-Donor or Multiple-Acceptor Components. *Adv. Mater.* **2018**, *30*, 1705706.
- (37) Gasparini, N.; Salleo, A.; McCulloch, I.; Baran, D. The Role of the Third Component in Ternary Organic Solar Cells. *Nat. Rev. Mater.* **2019**, *4*, 229–242.
- (38) Fu, H.; Wang, Z.; Sun, Y. Advances in Non-Fullerene Acceptor Based Ternary Organic Solar Cells. *Sol. RRL* **2018**, *2*, 1700158.
- (39) Xu, W.; Gao, F. The Progress and Prospects of Non-Fullerene Acceptors in Ternary Blend Organic Solar Cells. *Mater. Horizons* **2018**, *5*, 206–221.
- (40) Xie, Y.; Yang, F.; Li, Y.; Uddin, M. A.; Bi, P.; Fan, B.; Cai, Y.; Hao, X.; Woo, H. Y.; Li, W.; et al. Morphology Control Enables Efficient Ternary Organic Solar Cells. *Adv. Mater.* **2018**, *30*, 1803045.
- (41) Xiao, L.; He, B.; Hu, Q.; Maserati, L.; Zhao, Y.; Yang, B.; Kolaczkowski, M. A.; Anderson, C. L.; Borys, N. J.; Klivansky, L. M.; et al. Multiple Roles of a Non-Fullerene Acceptor Contribute Synergistically for High-Efficiency Ternary Organic Photovoltaics. *Joule* **2018**, *2*, 2154–2166.
- (42) Liu, L.; Liu, Q.; Xiao, Z.; Yang, S.; Yuan, Y.; Ding, L. Induced J-Aggregation in Acceptor Alloy Enhances Photocurrent. *Sci. Bull.* **2019**, *64*, 1083–1086.
- (43) Xiao, Z.; Jia, X.; Ding, L. Ternary Organic Solar Cells Offer 14% Power Conversion Efficiency. *Sci. Bull.* **2017**, *62*, 1562–1564.

- (44) Nian, L.; Kan, Y.; Wang, H.; Gao, K.; Xu, B.; Rong, Q.; Wang, R.; Wang, J.; Liu, F.; Chen, J.; et al. Ternary Non-Fullerene Polymer Solar Cells with 13.51% Efficiency and a Record-High Fill Factor of 78.13%. *Energy Environ. Sci.* **2018**, *11*, 3392–3399.
- (45) Song, X.; Gasparini, N.; Nahid, M. M.; Paleti, S. H. K.; Wang, J.-L.; Ade, H.; Baran, D. Dual Sensitizer and Processing-Aid Behavior of Donor Enables Efficient Ternary Organic Solar Cells. *Joule* **2019**, *3*, 846–857.
- (46) Li, S.; Ye, L.; Zhao, W.; Zhang, S.; Mukherjee, S.; Ade, H.; Hou, J. Energy-Level Modulation of Small-Molecule Electron Acceptors to Achieve over 12% Efficiency in Polymer Solar Cells. *Adv. Mater.* **2016**, *28*, 9423–9429.
- (47) Feng, H.; Song, X.; Zhang, Z.; Geng, R.; Yu, J.; Yang, L.; Baran, D.; Tang, W. Molecular Orientation Unified Nonfullerene Acceptor Enabling 14% Efficiency As-Cast Organic Solar Cells. *Adv. Funct. Mater.* **2019**, <https://doi.org/10.1002/adfm.201903269>.
- (48) Li, W.; Yan, Y.; Gong, Y.; Cai, J.; Cai, F.; Gurney, R. S.; Liu, D.; Pearson, A. J.; Lidzey, D. G.; Wang, T. Contrasting Effects of Energy Transfer in Determining Efficiency Improvements in Ternary Polymer Solar Cells. *Adv. Funct. Mater.* **2018**, *28*, 1704212.
- (49) Sapsford, K. E.; Berti, L.; Medintz, I. L. Materials for Fluorescence Resonance Energy Transfer Analysis: Beyond Traditional Donor–Acceptor Combinations. *Angew. Chem. Int. Ed.* **2006**, *45*, 4562–4589.
- (50) Liu, F.; Zhao, W.; Tumbleston, J. R.; Wang, C.; Gu, Y.; Wang, D.; Briseno, A. L.; Ade, H.; Russell, T. P. Understanding the Morphology of PTB7:PCBM Blends in Organic Photovoltaics. *Adv. Energy Mater.* **2014**, *4*, 1301377.
- (51) Rivnay, J.; Jimison, L. H.; Northrup, J. E.; Toney, M. F.; Noriega, R.; Lu, S.; Marks, T. J.; Facchetti, A.; Salleo, A. Large Modulation of Carrier Transport by Grain-Boundary Molecular Packing and Microstructure in Organic Thin Films. *Nat. Mater.* **2009**, *8*, 952–958.
- (52) Mai, J.; Lau, T. K.; Li, J.; Peng, S. H.; Hsu, C. S.; Jeng, U. S.; Zeng, J.; Zhao, N.; Xiao, X.; Lu, X. Understanding Morphology Compatibility for High-Performance Ternary Organic Solar Cells. *Chem. Mater.* **2016**, *28*, 6186–6195.

- (53) Liao, H. C.; Tsao, C. S.; Lin, T. H.; Chuang, C. M.; Chen, C. Y.; Jeng, U. S.; Su, C. H.; Chen, Y. F.; Su, W. F. Quantitative Nanoorganized Structural Evolution for a High Efficiency Bulk Heterojunction Polymer Solar Cell. *J. Am. Chem. Soc.* **2011**, *133*, 13064–13073.
- (54) Xiao, Y.; Lu, X. Morphology of Organic Photovoltaic Non-Fullerene Acceptors Investigated by Grazing Incidence X-Ray Scattering Techniques. *Mater. Today Nano* **2019**, *5*, 100030.
- (55) Pan, F.; Zhang, L.; Jiang, H.; Yuan, D.; Nian, Y.; Cao, Y.; Chen, J. As-Cast Ternary Polymer Solar Cells Based on a Nonfullerene Acceptor and Its Fluorinated Counterpart Showing Improved Efficiency and Good Thickness Tolerance. *J. Mater. Chem. A* **2019**, *7*, 9798–9806.
- (56) Jiang, H.; Li, X.; Liang, Z.; Huang, G.; Chen, W.; Zheng, N.; Yang, R. Employing Structurally Similar Acceptors as Crystalline Modulators to Construct High Efficiency Ternary Organic Solar Cells. *J. Mater. Chem. A* **2019**, *7*, 7760–7765.
- (57) Yiu, A. T.; Beaujuge, P. M.; Lee, O. P.; Woo, C. H.; Toney, M. F.; Fréchet, J. M. J. Side-Chain Tunability of Furan-Containing Low-Band-Gap Polymers Provides Control of Structural Order in Efficient Solar Cells. *J. Am. Chem. Soc.* **2012**, *134*, 2180–2185.
- (58) Zheng, Z.; Awartani, O. M.; Gautam, B.; Liu, D.; Qin, Y.; Li, W.; Bataller, A.; Gundogdu, K.; Ade, H.; Hou, J. Efficient Charge Transfer and Fine-Tuned Energy Level Alignment in a THF-Processed Fullerene-Free Organic Solar Cell with 11.3% Efficiency. *Adv. Mater.* **2017**, *29*, 1604241.
- (59) Scharber, M. C.; Mühlbacher, D.; Koppe, M.; Denk, P.; Waldauf, C.; Heeger, A. J.; Brabec, C. J. Design Rules for Donors in Bulk-Heterojunction Solar Cells—Towards 10 % Energy-Conversion Efficiency. *Adv. Mater.* **2006**, *18*, 789–794.
- (60) Xie, Y.; Zhou, W.; Yin, J.; Hu, X.; Zhang, L.; Meng, X.; Ai, Q.; Chen, Y. Post-Annealing to Recover the Reduced Open-Circuit Voltage Caused by Solvent Annealing in Organic Solar Cells. *J. Mater. Chem. A* **2016**, *4*, 6158–6166.